Magnetism and magnetization dynamics in thin film ferromagnets

Verhagen, T.G.A.

CHAPTER 2

Theory

Many physical phenomena in condensed matter physics, such as the Hall effect and the quantized conductance, can be explained well considering electrons as spinless particles with a charge $-e$. However, there are effects that cannot be described without taking the spin of the electron into account, such as magnetism [20, 21], the Kondo effect [22] and the spin Hall effect [23].

Spin is the intrinsic angular momentum of an electron, which is characterized with the spin quantum number s, which is $\frac{1}{2}$ for an electron. The spin angular momentum operator $\mathbf{S}$ is given by

$$\mathbf{S} = \frac{1}{2}\hbar\boldsymbol{\sigma}, \tag{2.1}$$

where $\hbar$ is the reduced Planck constant and $\boldsymbol{\sigma}$ are the Pauli spin matrices

$$\sigma_x = \begin{pmatrix} 0 & 1 \\ 1 & 0 \end{pmatrix}, \qquad \sigma_y = \begin{pmatrix} 0 & -i \\ i & 0 \end{pmatrix}, \qquad \sigma_z = \begin{pmatrix} 1 & 0 \\ 0 & -1 \end{pmatrix}. \tag{2.2}$$

In particular, when the spin is pointing along the z-axis, the corresponding eigenstates are $|\uparrow\rangle = \begin{pmatrix} 1 \\ 0 \end{pmatrix}$ and $|\downarrow\rangle = \begin{pmatrix} 0 \\ 1 \end{pmatrix}$ and the spin points either parallel (spin-up) or antiparallel (spin-down) to the z-axis.

The electron spin also possesses a magnetic moment $\boldsymbol{\mu}_s$

$$\boldsymbol{\mu}_s = -\frac{g\mu_B}{\hbar}\mathbf{S}, \tag{2.3}$$

where g is the g-factor equalling 2 for a free electron and μ_B is the Bohr magneton.

2.1 Magnetism

Magnetic properties are closely related to the electronic structure of the solid. Three different forms of magnetic states can be distinguished: diamagnetic, paramagnetic and magnetically ordered systems (e.g. ferromagnets or antiferromagnets) [20, 21]. While a (weak) diamagnetic contribution to the total magnetic susceptibility is present in all materials, paramagnetism or magnetic ordering can be observed only in materials with incomplete electron shells.

Diamagnetism

In a diamagnet, the action of an external magnetic field on the electrons moving in the orbitals induces a magnetic moment, which opposes the applied magnetic field (Lenz's law). Another contribution, Landau diamagnetism, originates from the Lorentz force acting on conduction electrons, which is, however, overshadowed by stronger Pauli paramagnetic contribution. Diamagnetism is in general a very weak phenomenon.

Paramagnetism

In atoms (ions) with incomplete atomic shells, the magnetic moment μ is proportional to the total angular momentum $\mathbf{L}$ + $\mathbf{S}$. Without an applied magnetic field, the magnetic moments point in a random direction if the interaction between the moments is negligible. In that case, the magnetic susceptibility χ is strongly temperature dependent and follows the Curie law $\chi = C/T$.

In itinerant electron systems, the state of the electrons can be described as a non-interacting gas of free electrons characterized by the momentum $\mathbf{k}$ and the spin $\boldsymbol{\sigma}$ of the valence electrons. When a magnetic field H is applied, the electron band is split into two spin subbands, where the energy of an electron is raised or lowered by $\frac{1}{2}g\mu_B H$ depending on the orientation of the spin, as is shown in Figure 2.1.a. The Pauli magnetic susceptibilty χ_P of this non-interacting gas of free electrons is then equal to [24]

$$\chi_P = \frac{M}{H} = 2\mu_B^2 N(E_F), \tag{2.4}$$

with M is the magnetization and $N(E_F)$ the density of states (DOS) at the Fermi energy.

Magnetically ordered systems - ferromagnetism

When the interaction between the moments is strong enough, the material exhibits magnetic ordering below a characteristic temperature, the Curie temperature T_C in ferromagnets or the Néel temperature T_N in antiferromagnets. In ferromagnets, the exchange interactions lead to parallel ordering of magnetic moments giving rise to non-zero magnetization already in zero magnetic field.

In the Stoner model for itinerant ferromagnets, the exchange interaction is treated in simplified form as a molecular field term with the Stoner exchange factor I as a measure for the interaction. All the spins feel an identical exchange field, which causes a splitting of the electron band into two spin subbands. The energy of the $n = n_\uparrow + n_\downarrow$ electrons is raised or lowered by $I\frac{n_{\uparrow(\downarrow)}}{n}$.

In the new state, the kinetic energy is increased as electrons originally occupying states with $k < k_F$ now occupy states with $k > k_F$. The increase in kinetic energy is compensated by a decrease in the Coulomb energy, as more spins are aligned and the total spatial overlap of electron states is reduced.

The susceptibility χ is then equal to

$$\chi_s = \frac{2\mu_B^2 N(E_F)}{1 - IN(E_F)}, \tag{2.5}$$

with I the Stoner exchange factor. When $IN(E_F)$ becomes larger than one, the susceptibility becomes negative, indicating that the interacting electron gas forms a spontaneous moment. For the transition metals, the Stoner exchange constants I are of comparable order (approximately 1 eV) and the transition to a ferromagnetic state depends mostly on the density of states at the Fermi energy. This implicates that narrow bands at the Fermi energy are needed that can give rise to a large DOS.

In a ferromagnetic material, the total energy is built up from (short range) exchange interactions and (long range) dipole fields, including shape and demagnetization effects. It is therefore usually energetically favourable to form magnetic domains to keep the magnetization inside the material and minimize the demagnetization fields. Each domain has a single orientation of the magnetization vector. In the absence of a magnetic field, the magnetization of a ferromagnet is close to zero.

With an increasing magnetic field, the amount of domains with a magnetization that is aligned with the applied field increases. When

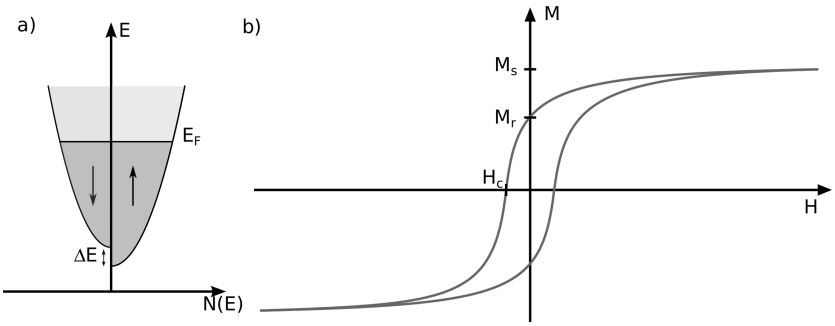

Figure 2.1: a) Density of states of an itinerant electron gas showing the splitting of the energy bands. b) The magnetization hysteresis loop for a ferromagnet. The saturation magnetization M_s is the maximum magnetization that can be obtained when all the magnetic moments are aligned, while the remanence or remanent magnetization M_r shows the magnetization of a ferromagnet when no external field is applied. The coercive field H_c is the opposite field needed to obtain zero magnetization.

the magnetization of all domains is aligned in the same direction, the maximum magnetization of the material is obtained: the saturation magnetization M_s. When the magnetic field is decreased to zero, the magnetization direction of the domains are not aligned all in the same direction and the remaining magnetization without an applied magnetic field is called the remanence or remanent magnetization M_r. The opposite magnetic field needed to drive the magnetization to zero is the coercive field H_c. Figure 2.1.b. shows an example of a magnetization hysteresis loop. Such a loop shows the magnetization of a ferromagnet as a function of an applied field.

2.2 Spin current

A key ingredient to describe spin transport properties are spin currents. A charge current $\mathbf{I_c}$ and spin current $\mathbf{I_s}$ are described as [25, 26]

$$\mathbf{I}_c = e\sum_{\mathbf{k}} \mathbf{v}_{\mathbf{k}\uparrow} f_{\mathbf{k}\uparrow} + \mathbf{v}_{\mathbf{k}\downarrow} f_{\mathbf{k}\downarrow}, \qquad \mathbf{I}_s = e\sum_{\mathbf{k}} \mathbf{v}_{\mathbf{k}\uparrow} f_{\mathbf{k}\uparrow} - \mathbf{v}_{\mathbf{k}\downarrow} f_{\mathbf{k}\downarrow}, \tag{2.6}$$

where $\mathbf{v}_{\mathbf{k}\sigma}$ is the velocity of an electron with momentum $\mathbf{k}$ and spin σ and $f_{\mathbf{k}\sigma}$ is the distribution function for electrons with momentum $\mathbf{k}$ and spin σ.

The distribution function $f_{\mathbf{k}\sigma}$ can be calculated using the Boltzmann transport equation [25, 26]

$$\mathbf{v}_{\mathbf{k}} \cdot \frac{f_{\mathbf{k}\sigma}}{\partial \mathbf{r}} + \frac{e}{\hbar}\mathbf{E} \cdot \frac{f_{\mathbf{k}\sigma}}{\partial \mathbf{k}} = \left(\frac{\partial f_{\mathbf{k}\sigma}}{\partial t}\right)_{\text{scattering}}, \tag{2.7}$$

where $\mathbf{E}$ is an external electric field. In many situations, the external fields produce only a small change $g_{\mathbf{k}\sigma}$ in the equilibrium distribution function $f^0_{\mathbf{k}\sigma}$. The scattering term can then be rewritten using the relaxation time approximation [25] as

$$\left(\frac{\partial f_{\mathbf{k}\sigma}}{\partial t}\right)_{\text{scattering}} = -\frac{g_{\mathbf{k}\sigma}}{\tau_\sigma} - \frac{f_{\mathbf{k}\sigma} - f_{\mathbf{k}-\sigma}}{\tau_{\text{sf}}}, \tag{2.8}$$

where τ_σ is the relaxation time for electrons with spin σ and τ_{sf} is the spin-flip time, that defines the time between two elastic collisions or two spin-flip collisions, respectively. The distance an electron ballistically travels between two collisions is the electron mean free path ℓ, which is equal to $\ell = v_F\tau_\sigma$, with v_F the Fermi velocity and the distance an electron ballistically travels between spin-flips is the spin-flip length ℓ_{sf}, which is equal to $\ell_{\text{sf}} = v_F\tau_{\text{sf}}$. A third length scale is the spin diffusion length $l_{\text{SD}} = \sqrt{D\tau_{\text{sf}}}$, with D the diffusion constant. The spin diffusion length is the distance the electron diffuses through the material between spin-flip collisions [27].

Using equation 2.6, three different types of current can be distinguished. When $\mathbf{v}_{\mathbf{k}\uparrow}f_{\mathbf{k}\uparrow} = \mathbf{v}_{\mathbf{k}\downarrow}f_{\mathbf{k}\downarrow}$, there is a pure charge current and no spin current is present. When $\mathbf{v}_{\mathbf{k}\uparrow}f_{\mathbf{k}\uparrow} = -\mathbf{v}_{\mathbf{k}\downarrow}f_{\mathbf{k}\downarrow}$, there exists a pure spin current and no charge current. In other cases, a spin polarized current with polarization P is present. The creation and the control of pure spin currents is a very attractive feature of spintronics, as it was argued by Murakami et al. [28] that pure spin currents have even time-reversal-symmetry. So, when time is reversed, both the direction of the current and spin are reversed and the spin current remains unchanged. In theory, devices can be constructed which carry pure and dissipationless spin currents, and which could thus overcome the major bottleneck when scaling down normal silicon based technology: heating.

2.3 Ferromagnetic heterostructures

During the last 30 years, the number of studies of heterostructures of ferromagnets (F) with normal metals (N), semiconductors (Sc) and superconductors (S) has grown impressively. Due to the discovery of

the Giant Magnetoresistance (GMR) effect at the end of the eighties by Baibich et al. [29] and Binasch et al. [30], the study between ferromagnets and normal metals became an area of intense fundamental and applied research. Nowadays the GMR effect is used in many products, ranging from magnetic sensors to magnetoresistive random-access memories (MRAM).

The GMR effect appears in thin films composed of alternating ferromagnetic and non-magnetic layers. The relative orientation of the magnetization direction of the ferromagnetic layers determines the resistance in the multilayer. Figure 2.2 shows a ferromagnet (F_1)/normal metal (N)/ferromagnet (F_2) trilayer, where the coercive field H_{c1} of layer F_1 is larger than the coercive field H_{c2} of layer F_2. A current that flows through layer F_1 becomes spin polarized. When the thickness of the N layer is smaller than the spin diffusion length, the spin polarized current will reach layer F_2. For simplicity, we assume that both layers are 100% spin polarized and all the electrons are either transmitted or reflected at the interface of layer F_2. When the magnetization of layer F_2 is parallel to F_1, all electrons can be transmitted (Figure 2.2.a) through F_2 and a current will flow through the trilayer. When the magnetization of layer F_2 is antiparallel to layer F_1, all electrons are reflected off F_2 (Figure 2.2.b) and no current will flow through the trilayer. The resulting resistance as a function of the applied external field H, the magnetoresistance, is plotted in Figure 2.2.c. The fixed F_1 layer and free F_2 layer behave different to the applied external magnetic field and the magnetization direction switches at a different applied field, H_{c1} and H_{c2} respectively.

The transport properties through GMR devices with ferromagnets with spin polarization P and where both ferromagnetic layers have a collinear magnetization, where the magnetization is aligned with the spin quantization axis, can be described using the two-channel series resistor model that was introduced by Valet and Fert [31]. In the Valet-Fert model, the total current is modelled as two individual currents for the spin-up and spin-down channel, limited by a channel dependent resistances that represent the bulk and interface scattering.

The attraction of the interaction between ferromagnets and normal metals lies in the fact that already at room temperature large effects can be observed. Theoretically, they can be explained well using the framework of static magnetoelectronic circuit theory [32]. This theory describes the charge and spin transport in multilayers by dividing the device in a circuit with reservoirs, resistors and nodes. An important contribution here comes from the interface. For a collinear magnetization, the spin dependent interface conductance, $G^{\uparrow(\downarrow)}$, is given by the

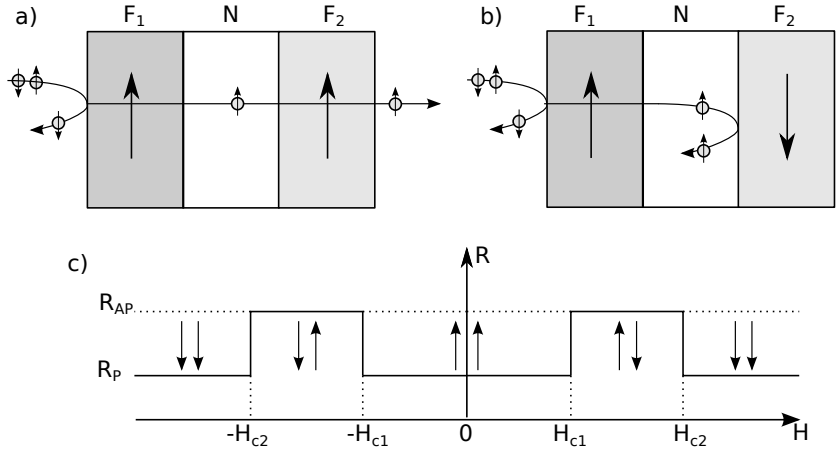

Figure 2.2: Giant magnetoresistance in a ferromagnet (F_1)/normal metal (N)/ferromagnet (F_2) trilayer. The incoming unpolarized electrons from the left side are polarized by the F_1 layer. Depending on the orientation of the magnetization of the F_2 layer with respect to F_1, the electrons are either fully transmitted (a) or reflected (b). In (c), the resistance of the $F_1/N/F_2$ trilayer is shown as a function of the applied field H. The magnetization direction of the F_1 and F_2-layer switches at different applied field (H_{c1} and H_{c2}). A higher resistance, R_{AP}, occurs when the magnetization in the ferromagnetic layers is in the antiparallel ($\uparrow\downarrow$ or $\downarrow\uparrow$) state and a lower resistance, R_P, occurs when the magnetization in F_1 and F_2 is in a parallel ($\uparrow\uparrow$ or $\downarrow\downarrow$) state.

Landauer-Büttiker formula in a two-spin channel model and is equal to

$$G^{\uparrow(\downarrow)} = \frac{e^2}{h} \sum_{nm} \left| t_{nm}^{\uparrow(\downarrow)} \right|^2, \tag{2.9}$$

where $\left| t_{nm}^{\uparrow(\downarrow)} \right|^2$ is the probability that a spin-up(spin-down) electron in mode n is transmitted at the interface as a spin-up(spin-down) electron in mode m. For transport between non-collinear ferromagnets, also the spin-mixing conductance $G^{\uparrow\downarrow}$ should be taken into account [33]. It is equal to

$$G^{\uparrow\downarrow} = \frac{e^2}{h} \left[M - \sum_{nm} r_{nm}^{\uparrow} \left(r_{nm}^{\downarrow} \right)^* \right], \tag{2.10}$$

where M is the total number of transport channels and $r_{nm}^{\uparrow(\downarrow)}$ are the reflection coefficients between transport channels n and m. The spin-mixing conductance is a complex quantity, where the product $r_{nm}^{\uparrow}\left(r_{nm}^{\downarrow}\right)^{*}$ describes the angle between the incoming spin-up electron and reflected spin-down electron at a normal metal/ferromagnet interface [34].

2.4 Magnetization dynamics

A shift from studying the static to the dynamical properties of ferromagnetic-normal metal multilayers was initiated by Berger [12] and Slonczewski [13] in 1996, who proposed that electric currents can induce a reorientation of the magnetization direction in multilayer structures, by the spin transfer torque (STT) mechanism. Already two years later, Tsoi et al. [35] demonstrated that when injecting a very high current density, order of 10^{12} A/m^2, using a point contact into $(\mathrm{Co/Cu})_N$ multilayers, magnetization precession can be induced. In 1999, Myers et al. [36] showed that when injecting a very high current density via a lithographic point contact into a Co/Cu/Co multilayer, the orientation of a magnetic domain in the Co layer can be switched. The subsequent discovery of Kiselev et al. [37] that the STT leads to a persistent oscillation at the gigahertz range in a Cu/Co/Cu/Co/Cu/Pt nanopillar opened the field of high frequency detection and manipulation of dynamical STT effects.

2.4.1 Landau-Lifshitz-Gilbert equation of motion

In ferromagnets, the magnetic moments are coupled via the exchange interaction. Therefore, the whole spin system with magnetization $\mathbf{M}$ can be considered as one macrospin. The dynamics of this macrospin is usually described by the phenomenological Landau-Lifshitz-Gilbert (LLG) equation of motion [38–41]

$$\frac{d\mathbf{m}}{dt} = -\gamma \mathbf{m} \times \mathbf{H}_{\text{eff}} + \alpha \mathbf{m} \times \frac{d\mathbf{m}}{dt} + \boldsymbol{\tau}, \tag{2.11}$$

where $\mathbf{m} = \frac{\mathbf{M}}{|\mathbf{M}|}$ is the unit direction vector of the magnetization $\mathbf{M}$, γ the gyromagnetic ratio, which is defined as $\gamma = g\mu_B/\hbar > 0$, $\mathbf{H}_{\text{eff}}$ is the local effective magnetic field including the external, demagnetization and crystal anisotropy fields, α the dimensionless Gilbert damping, with a typical intrinsic value of $\alpha_0 \approx 10^{-3}$ - 10^{-2} for transition-metal ferromagnets [42] and $\boldsymbol{\tau}$ accounts for the extra torques present in the system that are induced due to either current and/or spin orbit effects.

The parameter α is sometimes also encountered as the Gilbert parameter $G = \alpha\gamma M_s$. Note that, since $\mathbf{m}$ is a unit direction vector, the LLG equation describes transverse magnetization dynamics. The first term on the right side of equation 2.11 describes how the magnetization precesses around the local effective field $\mathbf{H}_{\text{eff}}$ at the Larmor frequency $\boldsymbol{\omega_L} = \gamma\mathbf{H}_{\text{eff}}$. The second term describes how the magnetization spirals down on a time scale $(\alpha\omega)^{-1}$ to this local effective field.

2.4.2 Spin-transfer torque

A more general description for the GMR effect described in section 2.3 takes into account that the magnetization direction of both magnetic layers does not need to be collinear. In Figure 2.3.a, a $F_1/N/F_2$ trilayer is shown where the angle between the magnetization of the F_2 and F_1 layer is equal to θ and the magnetization in F_2 is aligned with the spin quantization axis. The resistance is used to monitor the orientation of the magnetization between the two ferromagnetic layers of the trilayer.

When an electron flows through layer F_1, where the magnetization is not aligned with the spin quantization axis, the state of the electron is a superposition of the spin-up $|\uparrow\rangle$ and spin-down $|\downarrow\rangle$ state. The $|\uparrow\rangle$-state can cross the interface between N and F_2 and the $|\downarrow\rangle$ state is reflected. Comparing the angular momentum of the electron before and after the scattering process shows that angular momentum is absorbed by the magnetization of the ferromagnet F_2 within the transverse magnetic coherence length [43]

$$\lambda_c = \frac{\pi}{|k_\uparrow^F - k_\downarrow^F|}, \tag{2.12}$$

where $k_{\uparrow(\downarrow)}^F$ are the spin-up and spin-down Fermi wave vectors. In the transition metal ferromagnets Co, Fe and Ni, the transverse magnetic coherence length is in the order of a few Ångström (a tenth of a nm).

A non-collinear spin current can be decomposed in three polarization components: parallel to the magnetization; perpendicular to the magnetization and spin-current, $\mathbf{I}_s \times \mathbf{M}$, the so-called field-like torque $\boldsymbol{\tau}_{\text{FLT}}$; or parallel to the spin-current, $\mathbf{M} \times (\mathbf{I}_s \times \mathbf{M})$, the spin-transfer torque $\boldsymbol{\tau}_{\text{STT}}$. The total torque $\boldsymbol{\tau}$ that acts on the magnetization is then [32]

$$\begin{aligned}\boldsymbol{\tau} &= \boldsymbol{\tau}_{\text{STT}} + \boldsymbol{\tau}_{\text{FLT}} \\ &= -\frac{\hbar}{e}\text{Re}(G^{\uparrow\downarrow})\mathbf{m} \times (\boldsymbol{\mu} \times \mathbf{m}) - \frac{\hbar}{e}\text{Im}(G^{\uparrow\downarrow})\boldsymbol{\mu} \times \mathbf{m},\end{aligned} \tag{2.13}$$

with $\boldsymbol{\mu}$ the total spin-accumulation in the adjacent normal metal. It should be no surprise that both $\boldsymbol{\tau}_{\text{STT}}$ and $\boldsymbol{\tau}_{\text{FLT}}$ are determined by the

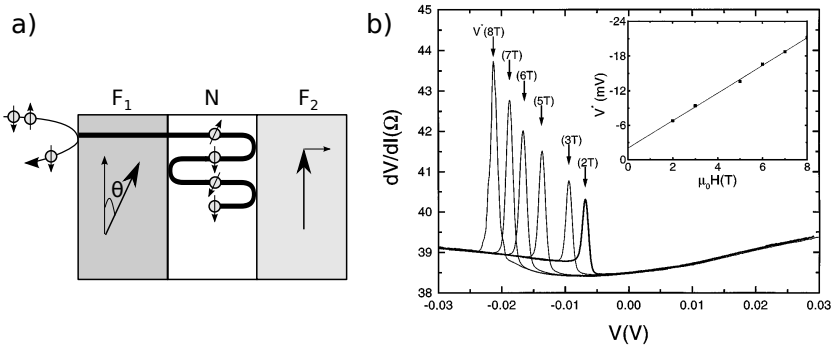

Figure 2.3: a) Spin transfer torque in a $F_1/N/F_2$ trilayer. The angle between the magnetization direction of layers F_1 and F_2 is equal to θ. The right moving electrons are polarized in the F_1 layer and will exert a torque on the magnetization in F_2. The reflected electron, whose polarization is antiparallel to F_2, will exert a torque on F_1. During each reflection, the electron exerts a torque on either F_1 or F_2, but the influence of higher order scatterings is small as the electron flux decreases with each scattering. b) Differential resistance as a function of the voltage bias for a mechanical point contact to a $(Co/Cu)_N$ multilayer, for different out-of-plane applied magnetic fields. The peaks in the differential resistance indicate the onset of the STT. The inset shows that the threshold current is a linear function of the applied magnetic field. Figure b) adapted from [35].

interface spin mixing parameter $G^{\uparrow\downarrow}$, given the smallness of the transverse coherence length λ_c.

For metallic systems, the STT is the dominant torque, as Re $(G^{\uparrow\downarrow})$ $\gg$ Im $(G^{\uparrow\downarrow})$ [44], and the field-like torque can be disregarded in many practical situations.

The change in magnetization due to the transfer of angular momentum of only one spin is very small, but when the current density $\mathbf{J}_c > 10^{10}$ A/m^2, the induced STT becomes of the same order as the magnetization.

In Figure 2.4, trajectories are plotted of the magnetization $\mathbf{M}$ in a free magnetic layer without anisotropies, that are a solution of the Landau-Lifshitz-Gilbert equation of motion. As shown in Figure 2.4.a, without damping and spin-transfer torque, the magnetization precesses in a circle due to the torque of the applied magnetic field. If there is also damping present in the system, after the magnetization is perturbed away

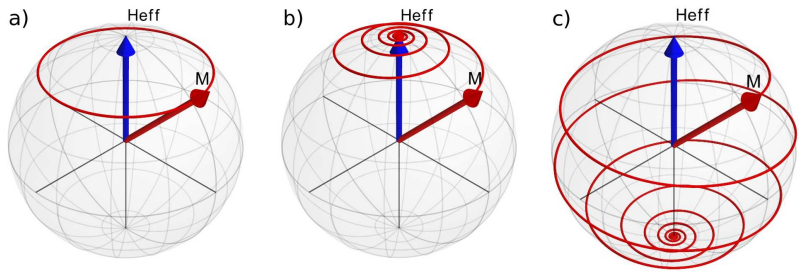

Figure 2.4: Precession of the magnetization in a free magnetic layer without anisotropy. In a), no Gilbert damping and STT is present and the magnetization precesses in a constant trajectory. When damping is introduced, the magnetization precesses slowly back until it is aligned with H_{eff} as shown in b). In c) a large STT is introduced that can switch the magnetization. Images adapted from [45]

from the equilibrium state, it will slowly spiral back until the magnetization is aligned with the local effective magnetic field as is shown in Figure 2.4.b. For a spin polarized current below some critical current, the STT acting on the magnetization is not large enough to change the magnetization direction. After the magnetization is perturbed, the magnetization will spiral back, until it is aligned with the local effective magnetic field. When the spin polarized current is larger than the critical current, the STT is large enough to change the magnetization direction and the magnetization spirals away to an equilibrium situation where the damping and the STT are in equilibrium, or the STT can even switch the magnetization direction direction as shown in Figure 2.4.c.

2.4.3 Spin-orbit torque

When an electron with momentum $\mathbf{k}$ is orbiting the nucleus, in the laboratory frame at rest it feels an electric field $\mathbf{E}$ from the nucleus. This electric field gives rise to a magnetic field $\mathbf{B}$ in the reference frame of the electron [46]. This magnetic field interacts with the spin of the electron and gives rise to the spin-orbit Hamiltonian $\mathcal{H}_{\text{SO}}$

$$\mathcal{H}_{\text{SO}} = -\frac{\hbar}{4m^2c^2}\boldsymbol{\sigma} \cdot \left(\hbar\mathbf{k} \times \nabla\tilde{\mathbf{V}}\right), \tag{2.14}$$

where m is the electron mass, c is the speed of light and $\tilde{\mathbf{V}}$ is the total potential. The total potential consist of a periodic crystal potential and a

potential due to local impurities, confinement, boundaries and external electrical fields [47].

Recently, van der Bijl and Duine [48] showed using linear-response matrix theory that when also the spin-orbit coupling is taken into account, a whole zoo of new current induced torques appear. As with the field-like-torque and the spin-transfer torque, these torques appear in pairs and have the form $\boldsymbol{\tau}^{\perp} = \mathbf{m} \times \boldsymbol{\tau}$. Some of these torques can be attributed to known physical effects like the inhomogeneous magnetization, the anisotropic magnetoresistance and the anomalous or spin Hall effect, but not all derived torques have a straightforward physical interpretation.

Spin-orbit torques can also be related to either structure inversion or bulk inversion asymmetry of the underlying structure, resulting in a Rashba or a Dresselhaus spin-orbit coupling, respectively. Well known systems where such a lack of bulk inversion symmetry can be found are semiconductors with the zinc blende structure such as (Ga,Mn)As [49–51] or crystals from the B20 space group such as FeGe [52] and MnSi [53] which shows a chiral spin-orbit interaction.

Recently, experiments and theory indicated that also in ultrathin metallic multilayers , Rashba spin-orbit coupling might be present. A static electric field $\mathbf{E} = E_0 e_z$ in the laboratory rest frame, where e_z points normal to the surface of the multilayers, produces a magnetic field $\mathbf{B} \propto k_x e_y - k_y e_x$ in the frame of the moving object, where $k_x e_y - k_y e_x$ is known as the Rashba spin-orbit coupling.

Experimentally, there is not yet agreement about the observations of a Rashba spin-orbit torque, that was measured by Miron et al. [14] and follow up experiments [54, 55]. In these experiments, magnetization switching of a very thin ferromagnetic layer is studied, driven by the current through the layer in the presence of spin-orbit torques. In all studies performed to date, the ferromagnetic layer has either been asymmetrically sandwiched between a heavy metal layer and an oxide layer, e.g. Pt/Co/AlO_x or Ta/CoFeB/MgO [14, 54–57] or in periodic crystals that lack inversion symmetry like (Ga,Mn)As [49–51].

Two different torques are found in these experiments; one torque is an even function of the direction of the magnetization $\mathbf{m}$ and the other is an odd function of the direction of the magnetization. The even torque,
$\mathbf{T}^{\text{even}} = T^{\text{even}} \mathbf{m} \times [(\hat{\boldsymbol{e}}_z \times \mathbf{E}) \times \mathbf{m}]$, where $\mathbf{E}$ is the applied electric field and $\hat{\boldsymbol{e}}_z$ is a unit vector perpendicular to the interface of the ferromagnetic heterostructure, is expected to be driven by the spin current due to the spin Hall effect (SHE), see below, in the heavy-metal layer [58, 59]. The odd torque,

$\mathbf{T}^{\text{odd}} = T^{\text{odd}}(\hat{\boldsymbol{e}}_z \times \mathbf{E}) \times \mathbf{m}$, is expected to originate from the effective magnetic field due to spin dependent scattering in combination with the Rashba interaction, which originates from the broken inversion symmetry in the ferromagnetic heterostructures.

2.4.4 Spin Hall effect

When a current is sent through a crystal or thin film and a magnetic field is applied normal to the current, a Hall voltage can be measured perpendicular to both the current and magnetic field [60]. In ferromagnetic materials, the Hall voltage consists of a contribution of the normal Hall effect and the anomalous Hall effect (AHE). When a current flows through a ferromagnet, the spin-orbit interaction gives rise to asymmetric scattering of the electrons. So, if the spin-up electrons have a larger probability to scatter to the left then the spin-down electrons have a larger probability to scatter to the right.

In 1971, Dyakonov and Perel [61, 62] predicted that the same mechanism responsible for the AHE, could cause a spin imbalance in a nonmagnetic material. The work was rediscovered in 1999 by Hirsch [15], who labelled this phenomenon as spin Hall effect (SHE).

In the SHE, a spin current $\mathbf{I}_s$ is generated transverse to a charge current $\mathbf{I}_c$, because the spin-orbit interaction causes an asymmetric scattering of the spin-up and -down electrons as shown in Figure 2.5. The spin current $\mathbf{I}_s$ is equal to

$$\mathbf{I}_s = \alpha_{\text{SHE}} \boldsymbol{\sigma} \times \mathbf{I}_c, \tag{2.15}$$

where α_{SHE} is a material dependent parameter characterizing the efficiency of the SHE. The spin-orbit interaction causing the SHE is also able to convert a spin current into a charge current by the inverse spin Hall effect (ISHE), where the charge current is equal to

$$\mathbf{I}_c = \alpha_{\text{SHE}} \mathbf{I}_s \times \boldsymbol{\sigma}. \tag{2.16}$$

The SHE and ISHE make a full-electric manipulation of spin possible, even without the use of magnetic materials. To obtain a large spin current, a large α_{SHE} is needed. Up to now, most experiments use heavy paramagnetic materials such as Pt and Pd, because the strength of the spin-orbit coupling and thus also α_{SHE} scales with Z^4, Z being the atomic number. Recently, it has been shown that a large SHE can also be obtained when Cu is doped with Bi impurities [63, 64] or when heavy transition metals are grown in a high resistive phases as β-Ta [57] and β-W [65]. Wang et al. [66] proposed that the SHE can also be induced into

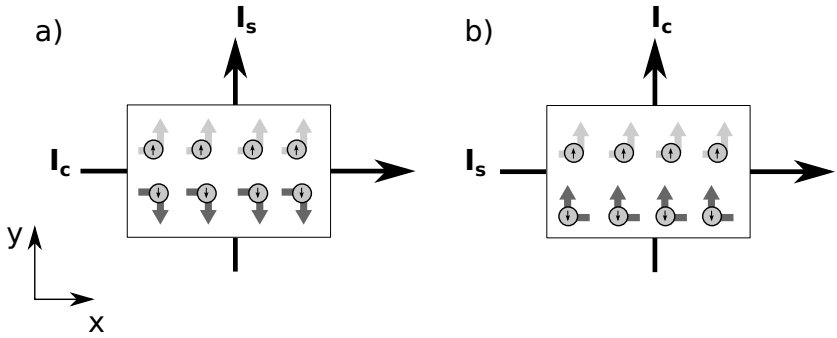

Figure 2.5: a) A spin current is induced by the spin Hall effect in a paramagnetic material. When sending a charge current in the x-direction, a spin current is generated in the y-direction due to the spin-orbit interaction. b) The inverse spin Hall effect induces a charge current in the y-direction when a spin current flows in the x-direction.

a thin normal metal when it is sandwiched between dissimilar insulators. The asymmetric interfaces break the inversion symmetry, which leads to a Rashba-type spin-orbit interaction. This spin-orbit interaction gives rise to a giant spin Hall conductivity.

2.4.5 Spin pumping

Where the spin transfer torque transfers angular momentum from a spin current to the magnetization of a ferromagnet, also the inverse process is possible. A precessing magnetization can emit an alternating spin current into an adjacent layer; a process called spin pumping, proposed by Berger [12] and Tserkovnyak [43, 67].

In Figure 2.6, spin pumping is schematically illustrated. In Figure 2.6.a, a ferromagnet in equilibrium is shown, where the density of states consists of a spin-up and spin-down band that are both filled up to the Fermi energy. If the magnetization of the ferromagnet is brought into a non-equilibrium state, the magnetization will relax by a spin-flip process of an electron above the Fermi energy into an empty state in the lower energy band. This process is called intrinsic damping [68, 69]. When there is an adjacent layer present, an additional relaxation process can occur. For ferromagnets that are thicker than the transverse coherence length, Tserkovnyak et al. [67] showed that the precessing

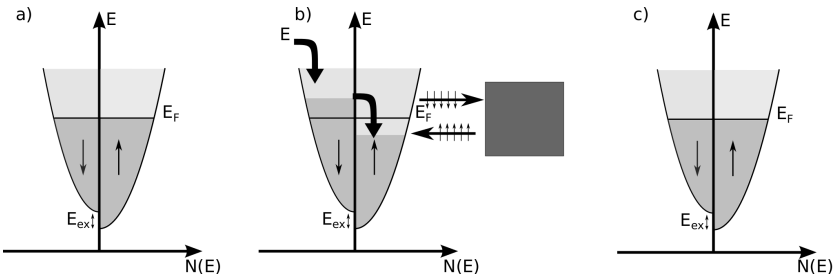

Figure 2.6: a) shows the Stoner model of a ferromagnet in equilibrium. Both the spin-up and -down band are filled up to the Fermi level E_F. They are shifted with respect to each other by the exchange energy E_{ex}. When the magnetization is brought into a non-equilibrium state (b), intrinsic relaxation can bring the ferromagnet back into equilibrium (c). When an adjacent layers is present, a spin current can be emitted into this layer to accelerate the relaxation (b). Adapted from [70].

magnetization emits a pure spin current

$$\mathbf{I}_s = \frac{\hbar}{4\pi}\left[\text{Re}(G^{\uparrow\downarrow})\mathbf{m}\times\frac{d\mathbf{m}}{dt} + \text{Im}(G^{\uparrow\downarrow})\frac{d\mathbf{m}}{dt}\right] \tag{2.17}$$

into the adjacent layer with a spin-flip probability ϵ. If the adjacent layer is a good spin sink, $\epsilon > 10^{-2}$, the spin current is efficiently absorbed, causing a decrease in the relaxation time. If the adjacent layer is a bad spin sink, $\epsilon < 10^{-2}$, no change in the magnetization dynamics will be observed. A bad spin sink can be turned into a good spin sink by doping it with spin-flip scatterers like heavy or magnetic impurities.

The spin-flip probability of a normal metals is mostly determined by the spin-orbit scattering. In normal metals, the spin-flip probability ϵ is equal to the ratio between the elastic and spin-orbit relaxation time, $\frac{\tau_{\text{el}}}{\tau_{\text{so}}}$. τ_{so} rapidly decreases with increasing Z and the spin sink effect becomes much more dominant with heavier elements such as Pt and Pd.

Furthermore, when the thickness d of the adjacent layer is smaller than the spin diffusion length l_{SD}, a spin accumulation is built up in the adjacent layer. Because the spins in the adjacent layer accumulate transverse to the magnetization of the ferromagnetic layer, the spin accumulation driven transport is described using the spin mixing conductance. Taking into account the spin accumulation, the spin mixing conductance $G^{\uparrow\downarrow}$ in equation 2.17 is replaced by an effective spin pump-

ing efficiency $A_{\text{eff}}^{\uparrow\downarrow}$ [43]

$$\frac{1}{A_{\text{eff}}^{\uparrow\downarrow}} = \frac{1}{G^{\uparrow\downarrow}} + \frac{R_{\text{sd}}}{\tanh(d/\lambda_{\text{SD}})}, \tag{2.18}$$

with R_{sd} is the resistance of the adjacent layer.

The extra damping α' and the possible modification of the gyromagnetic ratio γ due to spin pumping is equal to [43]

$$\alpha' = \frac{\gamma_{\text{eff}}}{\gamma}\left[\alpha + \frac{\hbar\gamma}{4\pi M_s A d_f}\text{Re}\left(A_{\text{eff}}^{\uparrow\downarrow}\right)\right], \tag{2.19}$$

where A is the area, d_f the thickness of the ferromagnet and γ_{eff} is the modified gyromagnetic ratio equal to [43]

$$\frac{\gamma}{\gamma_{\text{eff}}} = 1 - \frac{\hbar\gamma}{4\pi M_s A d_f}\text{Im}\left(A_{\text{eff}}^{\uparrow\downarrow}\right). \tag{2.20}$$

These two equations show that the spin pumping effect scales with $1/d_f$.

2.5 Spin-flip laser

In the previous sections we have seen what happens when a spin current flows from a normal metal into a ferromagnet. If the polarization of the spin current is non-collinear with the magnetization of the ferromagnet, the transverse component of the magnetization gives rise to a spin-transfer torque that can change the magnetization of the ferromagnet. Now, we will study what happens when a spin current is injected into a normal metal. Already in 1996, Berger [12] proposed that an injected current could excite spin waves in a ferromagnet. When injecting a spin current from a ferromagnet into a direct band semiconductor, it has been experimentally shown that circular polarized light can be emitted [71, 72]. In 2004, Kadigrobov [18, 19] proposed that when creating a non-equilibrium spin distribution in a normal metal or ferromagnet, there is a chance that this relaxes via a direct spin-flip transition and electromagnetic radiation is emitted. When it is possible to create a population inversion, even a spin-flip laser could be built. In 2006, Watts and van Wees [73] suggested that a MASER (Microwave Amplification by Stimulated Emission of Radiation) could be build when an external spin current is driven through a microwave created spin accumulation in a paramagnet.

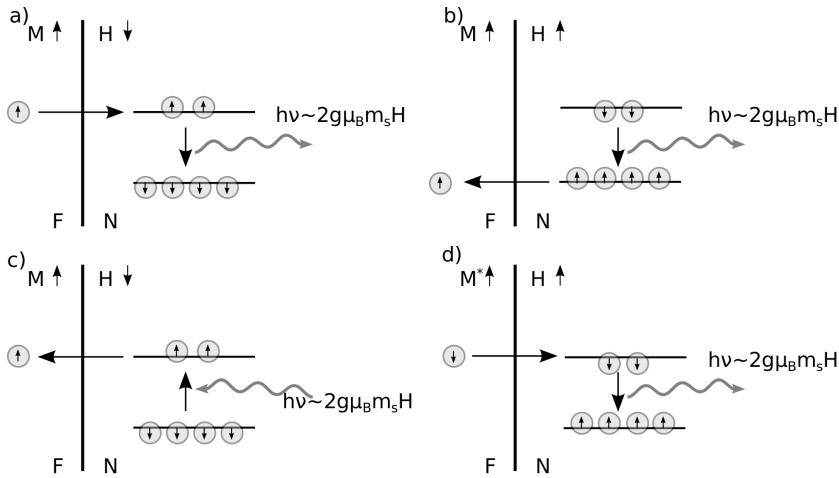

Figure 2.7: Four possible ferromagnet (F)/Normal metal (N) configurations, where a spin-flip process could generate a photon. In a), the magnetization M of F is antiparallel with the applied field H. Majority electrons are injected from F into N, leading to an inverse population of the Zeeman levels in N. A spontaneous or stimulated spin-flip process will emit a photon with the frequency proportional to the applied field H. b) When the magnetization M in F is parallel to the applied field H, electrons from the N layer are injected mostly in the majority band of F, resulting in an inversely populated Zeeman level in N. Again, a spontaneous or stimulated spin-flip process will emit a photon with the frequency proportional to the applied field H. In c), the magnetization M of F is antiparallel with the applied field H, but now the F/N bilayer is irradiated with photons with the energy equal to the Zeeman splitting. A spin-flip transition can be induced when a spin-down electron absorbs a photon. This will induce a photocurrent through the N into the F-layer. In d), the F layer is a minority type ferromagnet. When the magnetization M* is parallel to the applied field, minority carriers will flow from the F into the N layer, creating an inversely populated Zeeman level. Again, a spontaneous or stimulated spin-flip process will emit a photon with the frequency proportional to the applied field H. Adopted from [74].

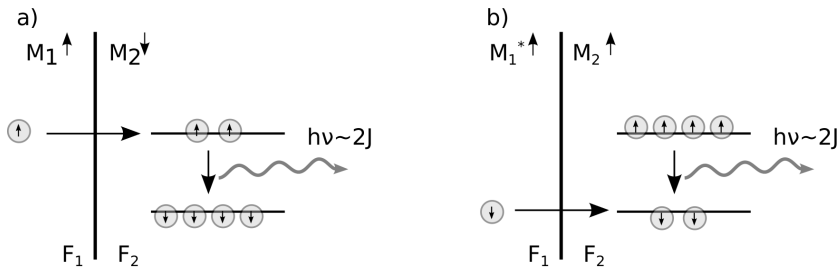

Figure 2.8: Two possible ferromagnet 1 (F_1)/ferromagnet 2 (F_2) configurations, where a spin-flip process could generate a photon. The normal metal layer is replaced with a second majority type (a) or minority type (b) ferromagnet respectively. Photons are generated in a similar way as in the F/N bilayer, but instead of splitting the energy states in a normal metal with the Zeeman energy, now a ferromagnet is used and the energy splitting is caused by the exchange energy J. Adapted from [74].

In Figure 2.7, four different configurations are shown that can be used to build a spin-flip laser from a normal metal/ferromagnetic bilayer. When an external magnetic field H is applied to a normal metal, the energy eigenstates are Zeeman split. When injecting electrons into the highest energy level or removing electrons from the lowest energy level, a population inversion can be induced into the normal metal layer. The relaxation of the population inversion requires spin-flip processes. In the case the spin-flip relaxation mechanisms in the normal metal is slow, so the normal metal should be a bad spin sink, a spin-flip process accompanied with the emission of a photon with frequency

$$h\nu = 2g\mu_B m_s H, \tag{2.21}$$

can increase the relaxation rate. For a normal metal with a g-value of 2, the emitted frequency is equal to 28 GHz/T.

As predicted by Berger [75], a voltage can be generated in a magnetic multilayer undergoing ferromagnetic resonance when a magnon is created or annilated by a spin-flip process. In Figure 2.7.c the inverse process is shown, where the ferromagnet/normal metal bilayer is irradiated with photons and a photocurrent is induced through the bilayer.

When replacing the normal metal with a weak ferromagnet, no external field is needed to split the energy levels. In Figure 2.8, two options are shown how a ferromagnet (F_1)/ferromagnet (F_2) spin-flip

lasers can be built. Again, by injection or removing electrons, a population inversion can be created in F_2, that can relax using a spin-flip relaxation with the emission of a photon with frequency

$$h\nu = 2J, \tag{2.22}$$

where J is the exchange energy of F_2. For a ferromagnet, the exchange energy can be tuned from a few meV for weak ferromagnets up to a few eV for the strong ferromagnets. Since 1 eV would corresponds to 500 THz, a very broad frequency range can be obtained with a spin-flip laser.